Appl Magn Reson (2015) 46:693–707
DOI 10.1007/s00723-015-0686-z

Applied
Magnetic Resonance

REVIEW

A Review of EPR Studies on Magnetization of Nanoparticles of Dilute Magnetic Semiconductors Doped by Transition-Metal Ions

Sergey I. Andronenko[1] · Sushil K. Misra[2]

Received: 31 December 2014 / Revised: 7 March 2015 / Published online: 19 April 2015

Abstract This article reviews recent electron paramagnetic resonance (EPR) studies on the magnetic properties of nanoparticles of dilute magnetic oxide semiconductors (DMS) doped with transition-metal ions. These nanoparticles are SnO_2 doped with Co^{2+}, Fe^{3+}, Cr^{3+} ions, CeO_2 doped with Ni^{2+}, Co^{2+} ions, and ZnO doped with Fe^{3+} ions. The EPR studies reveal that the method of synthesis, surface properties, and size of nanoparticles are important factors that determine the magnetic properties of DMS nanoparticles. In addition, they indicate that ferromagnetic and paramagnetic phases may coexist. The saturation magnetization, as estimated from EPR signal, depends both on the doping level of impurities and annealing temperature. Undoped DMS also exhibit ferromagnetism due to oxygen vacancies. Furthermore, the EPR spectrum depends very sensitively on the size of nanoparticle.

1 Introduction

Nanoparticles of oxides of transition and rare-earth metals, doped with 0.1–5 % transition-metal cations [1–4], are magnetic semiconductors, which possess all the properties required for their being exploited as spintronic devices, wherein the spins and charge carriers are strongly bound: they are ferromagnetic above room temperature; they possess rather high saturation magnetization; they are semiconductors, belonging, in general to V-type of half-metals [1], whose polarization of charge carriers is almost 100 % that for half-metals. Tin dioxide (SnO_2) is very

✉ Sushil K. Misra
sergey.andronenko@gmail.com; skmisra@alcor.concordia.ca

[1] Institute of Physics, Kazan Federal University, 18 Kremlevskaya str., Kazan 420008, Russia

[2] Physics Department, Concordia University, 1455 de Maisonneuve Boulevard West, Montreal, QC H3G 1M8, Canada

attractive system for a large number of practical applications, being a chemically stable transparent oxide semiconductor with a wide energy gap ~3.6 eV. It was found that doping SnO_2 nanoparticles with transition-metal ions (Co, Cr, Fe, Ni) induces ferromagnetism in them [5–15], rendering this compound a suitable ferromagnetic semiconductor at room temperature. Similarly, CeO_2 and ZnO are also suitable ferromagnetic semiconductors.

There are many aspects of nanoparticles revealed by electron paramagnetic resonance (EPR). When the EPR lines become quite broad, showing the effect of ferromagnetism of the sample, it is called a ferromagnetic resonance (FMR) line. In particular, the annealing temperature used to fabricate nanoparticles, concentration of impurity ions, the substance used for encapsulation, Curie temperature, saturation magnetization, level of spin polarization of nanoparticles, are exploited for rendering them as spintronic materials. The important aspects in the interpretation of EPR spectra in oxide DMS nanoparticles are: (1) FMR signal, (2) correlation of the intensity of FMR signal with the static magnetization data; (3) simultaneous existence of FMR and EPR signals; (4) correlation of EPR signal as observed in an oxide nanoparticle, prepared under varying synthesis conditions, doping level, surfactant, and size of nanoparticles with that in a single crystal of the same material.

The reported EPR studies reveal that the magnetic properties of DMS oxide compounds depend on impurity ion concentration, annealing temperature, temperature of study [5–15]. The following features are noteworthy: (1) suppression of ferromagnetism above threshold impurity concentration, explained to be due to interstition, rather than substitution, of impurity ions. (2) Increase of saturation magnetization with increasing annealing temperature of the samples, with the maximum occurring at 600 °C; and (3) coexistence of ferromagnetic moment and localized magnetic moments.

SnO_2, CeO_2, and ZnO are transparent semiconductors with energy gaps of 3.6, 3.2 and 3.3 eV, respectively, which can be modified by introduction of different impurities up to 4 eV [16, 17].

Reproducibility of data on magnetic and electric properties is a very important consideration in developing new materials based on oxide compounds for their functional applications. These properties depend strongly on the method of synthesis, annealing temperature, and impurities that initiate creation of electrons or holes. Fabrication of semiconductors in which spins are correlated with charge carriers is an important step in the development of spintronic devices to be used in practice. Thus one should choose prospective compounds, which are characterized by higher saturation magnetization, associated with higher degree of spin polarization. To this end, EPR is capable of detecting micro-inclusions of impurity ions, which can significantly alter the magnetic properties of DMS.

This article reviews the magnetic properties, as revealed by the recent EPR studies of nanoparticles of DMS oxide semiconductors SnO_2, CeO_2, and ZnO, doped with transition-metal ions [7–15]. It would cover the relevant EPR data, synthesis, effect of size, doping, coexistence of paramagnetism and ferromagnetism, internal magnetic fields, and the origin of ferromagnetism.

2 Effect of Size on the Properties of Nanoparticles

During the synthesis to nanoparticle phase there occur significant changes in physical properties of the system. The size decreases successively in transition from single-crystal phase, with negligible amount of surface defects, to polycrystalline phase, wherein surface and inter-granular effects play important roles, and subsequently to nanoparticles, wherein the surface area, endowed with different structural defects, forms the main part of the nanoparticle. Ultimately, there exists no crystalline analog for such a nanosystem. In nanoparticle phase the properties of the surface, enriched with defects, become different from those of the core. There are two types of aggregates of nanoparticles: (1) nanopowders, wherein surface coating (encapsulation) protects surface structure, and (2) nano-grains, wherein inter-granular fillers, connecting individual grains, become important.

The properties of nanoparticles change as their size decreases below 50 nm [18] due to two effects. (1) The nanoparticle size affects the electronic structure due to quantum confinement effect. When the size decreases from $\sim$50 nm, e.g. for SnO_2-doped Fe_2O_3 nanoparticles the energy gap increases significantly from 3.9 to 4.5 eV [16], which modifies the EPR signal. The electronic structure of dilute DMS changes with nanoparticle size, which, in turn, implies a change in the EPR resonance fields due to localized moments and relaxation times, as that reported, e.g., for donor and acceptor centers in nanoparticles of Al-doped ZnO [19].

Nanoparticles of size $\sim$25–40 nm exhibit distinct EPR/FMR spectra from surface (ferromagnetic) and core (diamagnetic) regions. As the size is further reduced, there occurs a distribution of spin-Hamiltonian parameters (SHP) in medium-size ($\sim$7 nm) nanoparticles due to the distribution of defects and vacancies in the region intermediate to the surface and the core. Simulation of EPR spectrum, in this case can be done by overlapping various EPR spectra corresponding to a distribution of SHP, e.g., in the case of ZnO nanoparticles doped with Fe ion [14], as described below. For smaller nanoparticles (2.5–5 nm), ferromagnetic or superparamagnetic signals are observed only at high temperature. However, for them at liquid helium temperature, EPR lines are observed due to localized moments, whose shape is distorted because of a distribution of SHP and formation of exchange-coupled clusters [14].

3 Review of Relevant EPR Data on Nanoparticles of SnO_2, CeO_2 and ZnO Doped by Transition-Metal Ions

Nanoparticles of SnO_2 doped with Co, Fe and Cr ions, CeO_2 doped with Ni and Co ions, and ZnO doped with Fe ions have been investigated by EPR [5–15]. The details of synthesis, size, structure, maximum doping level for which ferromagnetism appears, and EPR frequencies of study are summarized in Table 1. It was found, that there is a threshold level of concentration of magnetic impurity ions, above which ferromagnetism of SnO_2 and CeO_2 nanoparticles disappears, as shown in Fig. 1.

Table 1 Synthesis method, size, structure, ferromagnetism, and characteristic of EPR spectra of the various nanoparticles reviewed in this paper

Sample: doping ion	Method of synthesis	Nanoparticle size (nm)	Corresponding crystal structure	Maximum concentration (x) for which ferromagnetism appears (%)	Coexistence of EPR/FMR spectra
SnO_2: Co	Sol–gel	60–20	Rutile P4/mnm (cassiterite)	1	EPR/FMR
SnO_2: Fe	Sol–gel	65–25	Rutile P4/mnm (cassiterite)	5	EPR/FMR
SnO_2: Cr	Sol–gel	70–40	Rutile P4/mnm (cassiterite)	2.5	EPR/FMR
CeO_2: Ni	Sol–gel nitrate	9–5	Fluorite Fm3 m	4	EPR/FMR
CeO_2: Ni	Sol–gel acetate	~7	Fluorite Fm3 m	5	EPR/FMR
CeO_2: Co	Sol–gel acetate	2.7–4.9	Fluorite Fm3 m	5	EPR/FMR
ZnO: Fe	Hydrothermal solvents: (1) diethylene glycol (2) ethanol	~7	Wurtzite $P6_3mc$		EPR/FMR

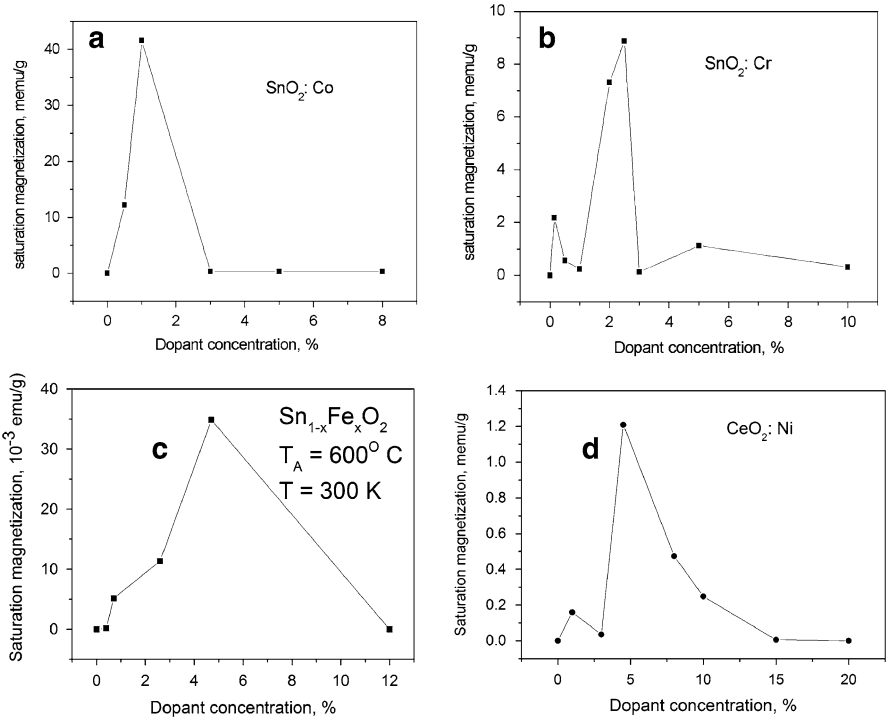

Fig. 1 Dependences of saturation magnetization of SnO_2 nanoparticles on the concentration of Co, Cr, Fe [6] and that of CeO_2 nanoparticles on the concentration of Ni [11]

The magnetic properties, as derived from EPR/FMR data for SnO_2, CeO_2, and ZnO have been reported in [1, 5, 6, 12, 13, 20, 21]. The relevant details are discussed below.

3.1 SnO_2

3.1.1 Co-Doped SnO_2

The Curie temperature of doped SnO_2 is below 850 K. Co doping of $\leq$1 % induces bulk ferromagnetism in SnO_2 nanoparticles. The size of nanoparticles varies with doping, from 6 nm (0 % Co) to 20 nm (8 % Co). EPR spectra of the Co^{2+} ion have been recorded at 5 K in chemically synthesized nanoparticles of SnO_2, annealed at 350 and at 600 °C, with Co concentrations of 0.5, 1, 3, 5 and 8 %. The spectra in the samples doped with $\leq$1 % cobalt can be simulated as a superposition of the spectra due to FMR and EPR lines, the latter belonging to low-spin ($S = 1/2$) Co^{2+} ions, in both substitutional and interstitional positions [7].

3.1.2 Fe-Doped SnO_2

Fe doping of $\leq$5 % induces ferromagnetism in SnO_2 nanoparticles. The size of nanoparticles varies from 65 nm (0 % doping) to 25 nm (5 % doping). The results on Fe^{3+} EPR investigations in $Sn_{1-x}Fe_xO_2$ nanoparticles doped with $0.00 \leq x \leq 0.05$ at X-band ($\sim$9.5 GHz) at different temperatures (5–300 K) were reported in [8]. The FMR line intensity indicated that the saturation magnetization depended on Fe concentration, as shown in Fig. 2, and also on the annealing temperature, as shown in Fig. 3 [12]. Similar results were also was reported for Co-doped SnO_2 nanoparticles. Magnetization of these samples, exhibiting ferromagnetic nature, is shown in Fig. 4. A high-frequency Fe^{3+} EPR study of nanoparticles of ferromagnetic semiconductor $Sn_{1-x}Fe_xO_2$, doped with $x = 0.005$, at room temperature, was carried out at 236 GHz (255 K) [9]. These EPR data show that Fe^{3+} spin-Hamiltonian parameters in these nanoparticles are close to those in single crystals.

3.1.3 Cr-Doped SnO_2

Cr doping ($\leq$2.5 %) induces ferromagnetism in SnO_2 nanoparticles. The size of nanoparticles varies from 70 nm (0 % doping) to 40 nm (5 % doping).

Cr^{3+} EPR spectra have been recorded at 5 K in SnO_2 nanoparticles, annealed at 600 °C with Cr concentrations of 0, 0.1, 0.5, 1, 1.5, 2.0, 2.5, 3.0, 5.0, 10 % [10]. Each spectrum can be simulated as a superposition of four magnetically inequivalent Cr^{3+} centers, characterized by different spin-Hamiltonian parameters. In addition, an FMR line appears due to surface ferromagnetism for the samples with Cr concentrations $\leq$2.5 %.

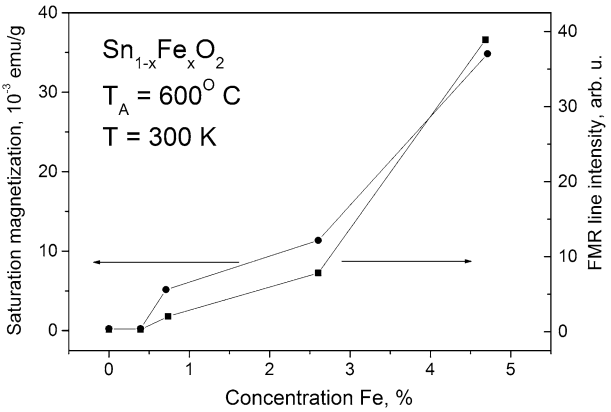

Fig. 2 Correlation of saturation magnetization and intensity of FMR line on Fe concentration [12]

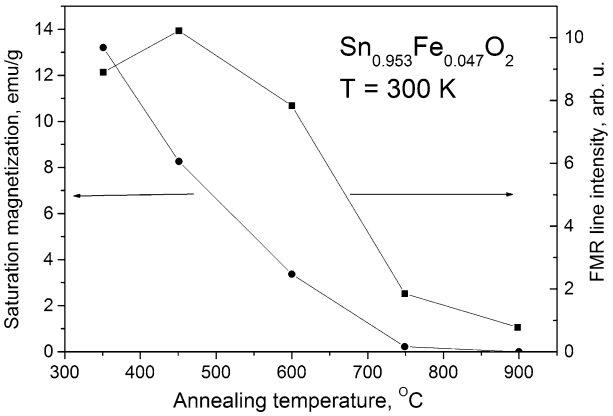

Fig. 3 Correlation of saturation magnetization and intensity of FMR line on annealing temperature [12]

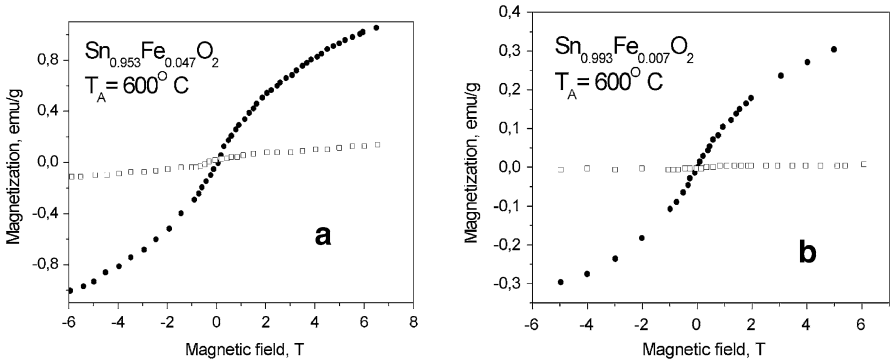

Fig. 4 Magnetization of SnO_2 nanoparticles doped with 4.7 % (**a**) and 0.7 % Fe (**b**) at 300 K [12]

3.2 CeO_2

3.2.1 Ni and Co-Doped CeO_2

Ni-doping of $\leq$4 % induces ferromagnetism in CeO_2 nanoparticles. Their EPR spectra were studied at 5 and 300 K [11] in CeO_2, doped with 1, 4, 8, and 10 % Ni, annealed at 500 °C. The size of nanoparticles varies from 9 nm (pure) to 5 nm (10 % Ni), depending on the annealing temperature. The Curie temperature varied for different doping, being below 600 K in each case. The magnetization of these samples is shown in Fig. 5. Detailed analysis of EPR spectra of various samples of $Ce_{1-x}Ni_xO_2$ doped with $0.01 \leq x \leq 0.10$, using rigorous simulation and fitting to experimental EPR spectra recorded at X-band ($\sim$9.39 GHz) at 5 and at 300 K, revealed the presence of several types of paramagnetic ions, as well as that of a FMR line from ferromagnetically ordered surface area [11]. Studies of these nanoparticles, using X-ray diffraction (XRD), X-ray photoelectron spectroscopy (XPS), thermogravimetry analysis (TGA), mass spectroscopy (MS) and investigation of magnetic properties, were reported in [13, 20].

In addition to the above, the samples of CeO_2 nanoparticles annealed at 200, 300, 400, and 500 °C, doped with 5 % Ni and 5 % Co ions were investigated by EPR at 4, 10 and 300 K and reported in [13]. The saturation magnetization versus annealing temperature is shown in Fig. 6. The size of these nanoparticles varies from 2.7 nm (annealing temperature 200 °C) to 4.9 nm (annealing temperature 500 °C), and it was from 5 to 9 nm for Ni-doped samples for different doping and annealing temperature [13, 20]. The EPR signals from Co^{2+} and Ni^{2+} ions were observed at 5 K, but only FMR spectra were observed at 300 K. There is also present a strong, narrow EPR signal ($g = 2.00$) in the samples, annealed at 200, 300, 400 °C, which was assigned to oxygen vacancies. The integrated intensity of EPR/FMR lines is

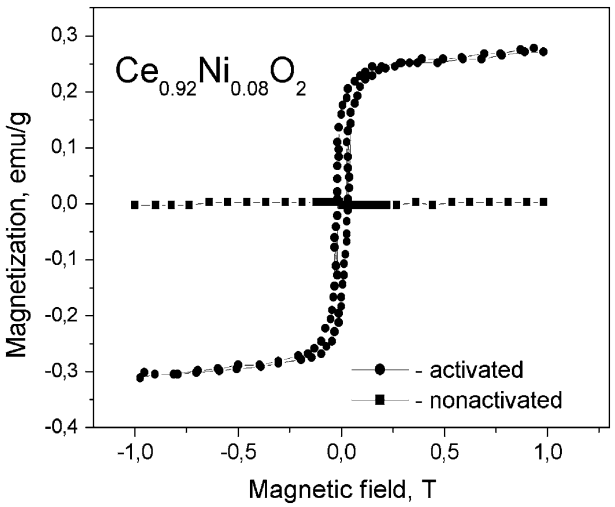

Fig. 5 Magnetization of CeO_2: Ni for annealed and annealed at 450 °C samples [20]

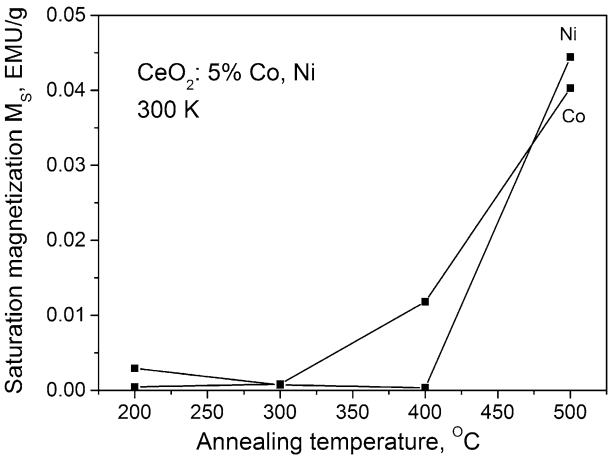

Fig. 6 Dependence of saturation magnetization of CeO_2: Co, Ni on annealing temperature [13]

proportional to the saturation magnetization. The intensity of the FMR signal in CeO_2 sample, doped with Co, increases with increasing annealing temperature. On the other hand, the intensity of the FMR signal in CeO_2 sample, doped with Ni, does not change much with annealing temperature. A strong superparamagnetic EPR signal appears in samples annealed above 400 °C. This signal is characterized by the *g* value about 2.0.

The number of oxygen vacancies, which contributes to the ferromagnetism of the sample, increases with annealing temperature. The saturation magnetization of CeO_2 samples, doped with Ni^{2+} and Co^{2+} ions, increases with annealing temperature above 400 °C, which can be explained to be due to the formation of oxygen vacancies.

3.3 ZnO

3.3.1 Fe-Doped ZnO

EPR studies on two types of nanoparticles of ZnO, NL and QJ, prepared using similar chemical hydrolysis methods in diethylene glycol and in denatured ethanol solutions, respectively, doped with 0.1–10 % Fe^{3+} have been reported at X-band (9.5 GHz) at 77 K and at Q-band (34 GHz) at 10, 80, 295 K [14]. The various $Zn_{1-x}Fe_xO$ nanoparticles investigated were of medium size, about 6.85 nm [21]. The simulation of EPR spectra for NL samples revealed that they contained three types of Fe^{3+} ions: (1) those, which substituted for Zn ions, exhibiting trigonal Fe^{3+} EPR spectrum in crystalline ZnO, the zero-field splitting (ZFS) parameter for which has a large distribution over the sample due to oxygen vacancies in the second coordination sphere; (2) those, which are characterized by very small ZFS; and (3) ferromagnetically (FM) ordered Fe ions in the samples with concentration of Fe more than 1 %.

The main conclusions of experimental EPR investigations of ZnO nanoparticles in NL and QJ samples are as follows: (1) the observed EPR spectra in NL samples with Fe concentration of more than 2.5 % indicate the presence of both paramagnetic Fe^{3+} ions exhibiting sharp lines, and ferromagnetically coupled Fe ions producing a single broad line; (2) the EPR spectrum for localized Fe^{3+} ions in NL sample were successfully interpreted by taking into account a Gaussian distribution of the zero-field splitting zfs (b_2^0) parameter. There were present two sets of EPR signals, HS1 and HS2, which became more intense with increasing Fe concentration; (3) the magnetic moment observed in NL samples is smaller, because the paramagnetic fraction of the doped ions does not contribute to the ferromagnetic coupling. QJ samples, on the other hand, only exhibit FM resonance signals, suggesting that all the doped Fe ions in them are magnetically coupled. This accounts for their stronger ferromagnetism.

3.3.2 ZnO Nanorods

The effect of reduced graphene capping on these samples as affecting ferromagnetism was investigated in detail in [15] by EPR, described as follows. Capping strongly affects the magnetic state of nanoparticles. The EPR spectra show that RGO (reduced graphene oxide) passivates singly charged oxygen vacancies (V_{OS}^{+}) in ZnO. It correlates the passivation efficiency of V_{OS}^{+} to the number of RGO layers, and this has been achieved up to 90 % by 31 layers of RGO. Due to passivation of V_{OS}^{+} in ZnO by RGO, the ferromagnetic behavior, that is the saturation magnetization and divergence between zero-field cooled and field cooling, in ZnO–RGO hybrids is suppressed as compared to that in ZnO. Combining the EPR and magnetic behaviors, a direct link between the passivation of singly charged oxygen vacancies present on the surface of ZnO nanorods and the number of RGO layers is established. It emphasizes the role of surface defects and surface passivation on the magnetic behavior of nanosized species of nanoparticles and nanorods.

3.3.3 ZnO Quantum Dots

Quantum dot is a nanocrystal, which is small enough to exhibit quantum mechanical properties. Intrinsic defects in dilute magnetic semiconductors determine their electrical and magnetic properties. Investigation of donor and acceptor centers in ZnO nanocrystals by EPR is, therefore, quite important, and many EPR studies have been reported [19, 22–27], described briefly as follows. It was found that Li and Na, which are components of commonly used compounds for ZnO nanoparticle synthesis, act as shallow donors, and are located in the core of ZnO nanoparticle [22]. It was found that ZnO nanoparticles effect dynamic spin polarization of ^{67}Zn and ^{1}H nuclear spins, being shallow donors [23]. On the other hand, H has also been found to act as a shallow donor, being located in $Zn(OH)_2$ capping shell covering the nanocrystal. In addition, Al, Ga, I also act as donors, whereas N acts as a shallow acceptor [19, 24]. The effect of electron confinement was investigated in n-type ZnO quantum dots, in which the g value changes from 1.960 to 1.968 for

nanoparticles with the sizes 3–7 nm [24]. Charge-controllable magnetism was observed in ZnO: Mn, in which the injection of electrons activates Mn^{2+}–Mn^{2+} ferromagnetic interaction [25]. EPR and ENDOR techniques are excellent tools for studying spatial distribution of the electronic wave function. This latter aspect is particularly interesting, because it allows for a quantitative measurement of the effect of confinement on the shape and properties of the wave function. This technique was successfully applied to Li- and Na-doped ZnO nanocrystals [26]. Co- and Mn-doped ZnO colloidal quantum dots are promising classes of diluted magnetic semiconductors, and have been investigated recently [27].

4 Origin of Ferromagnetism in Oxide Nanoparticles

The theory of ferromagnetism in DMS compounds is not yet fully developed. There is still a debate in the literature, whether itinerant ferromagnetism really exists in dilute magnetic semiconductors. Notwithstanding this, there are several mechanisms of ferromagnetism in DMS compounds, which have been proposed so far: (1) indirect exchange interaction between impurity transition-metal ions through oxygen ions (O^-) or oxygen vacancies [2]. The dependence of saturation magnetization on the number of oxygen vacancies was reported, in particular, in [28]. Oxygen vacancies on the surface of nanoparticles induce ferromagnetism even in undoped oxides [29–31]. As a modification of this approach, there are proposed: (2) indirect exchange interactions via magnetic polarons [3], and (3) interaction of impurity ions via color centers, which are oxygen vacancies with trapped electrons, also referred to as F-centers [4]; (4) defect-related mechanism for ferromagnetism in nanoparticles of DMS, based on charge transfer in defect oxides, as explained by the model of Stoner ferromagnetism [32].

There still remains some doubt on the nature of the ferromagnetic behavior of nanoparticles of oxides of Zn, Sn, Ce, Ti, doped with Fe, Cr, Co, Ni [2]. Some studies [33] deny the possibility of existence of itinerant (long-range) ferromagnetism in this system. Superparamagnetic behavior, with ferromagnetic interaction between paramagnetic ions, has been ascribed to the presence of nanoparticles of metallic Co or Co_2O_3 with very small size, 1–2 nm, as observed in ZnO nanoparticles [34]. Volbers et al. [35] did not find ferromagnetism in ZnO: Co nanoparticles. XRD technique is unable to detect any secondary phases for such small particles, and therefore they were not observed in the reported XRD pictures. On the other hand, many investigations suggest the existence of long-range ferromagnetic exchange interactions in ZnO: Co nanoparticles [36, 37]. Direct confirmation of such possibility was found in ZnO crystals doped with Co^{2+} ions, where Co^{2+}–Co^{2+} dimer centers were found, in which Co^{2+} ions are coupled with weak ferromagnetic interactions. This was explained by invoking the mechanism involving additional defects, e.g. singly charged oxygen vacancies [38]. Another possibility for the existence of ferromagnetically coupled Co^{2+} ions in this nanoparticle was reported in [39], where the competition between two groups of Co ions occurred, one with antiferromagnetic interaction between Co ions and the other with ferromagnetic interaction. Finally, there occurs superparamagnetic behavior,

with ferromagnetic interaction, in clusters of Co ions, and the magnetization behavior of nanoparticles of ZnO, doped with Co ions, is determined by the paramagnetic and superparamagnetic contributions.

5 Effect of Doping by Transition-Metal Ions on Saturation Magnetization

Saturation magnetization, which is proportional to the intensity of the FMR line, increases with increasing doping level of transition-metal ions, as seen from Fig. 1. However, above certain concentration of doping, there occurs a decrease and final quenching of saturation magnetization. The doping transition-metal ion substitutes for an Sn^{4+} ion or a Ce^{4+} ion, respectively, in SnO_2 and CeO_2, for low concentrations. But above certain concentration, this ion becomes introduced at interstitional positions, as concluded for Ni-doped CeO_2 [11]. This leads to a decrease in saturation magnetization. Adding more transition-metal ions does not contribute to ferromagnetism. On the other hand, it is possible to increase the saturation magnetization by annealing the samples at 600 °C, as seen from Fig. 5 for Ni^{2+}-doped CeO_2, which causes interstitional transition-metal ions to migrate to substitutional Sn^{4+} or Ce^{4+} ion positions [11]. A decrease of saturation magnetization with further doping may occur due to formation of antiferromagnetically coupled clusters.

6 Simultaneous Existence of Ferromagnetism and Localized Magnetic Moments

The broad FMR lines appearing at $g > 2.0$, in SnO_2 and CeO_2 [7, 8, 11–13] nanoparticles are due to transition-metal (TM) ions, which interact via the intermediary of magnetic color centers, i.e. F-centers, which consist of an oxygen vacancy trapped by an electron [4]. The FMR g value varies for SnO_2 for different dopant ions: $g = 4$ for Co, $g = 3.3$ for Fe, and $g = 2.7$ for Cr; whereas, for CeO_2 it changes: $g = 2.45$ for Ni, $g = 2.9$–4.0 for Co for samples prepared at different annealing temperatures. It appears that there exists some region near the surface of a nanoparticle in these materials, which has a rather increased concentration of oxygen vacancies, in which ferromagnetically coupled network, containing TM^{n+}–□–TM^{n+} groups are formed (□ denotes an oxygen vacancy), which exhibit an FMR line. There also exists some region in these nanoparticles which lacks oxygen vacancies, where TM ions are not coupled to each other via oxygen vacancies, which then exhibit only EPR, rather than FMR, signals. In this manner, EPR and FMR signals appear simultaneously within a nanoparticle, as confirmed for CeO_2 nanoparticles, doped with Co ions [13].

7 Internal Magnetic Fields: Shift of EPR Resonance Lines

There are mainly two sources, which cause shift in EPR resonance fields in nanosized oxides. These are: (1) ferromagnetically ordered regions on the surface of nanoparticle; and (2) paramagnetic or ferromagnetic particles surrounding a nanoparticle [40]. All these induce additional magnetic fields, which shift resonance line positions at the site of an impurity paramagnetic ion in the core area of a nanoparticle. These shifts explain the differences in EPR spectra of transition-metal ions, as observed in nanoparticles, from those in single crystals for the same chemical compounds, e.g., in nanoparticles of SnO_2, doped with Fe^{3+} [8] or Cr^{3+} ions [10].

8 Dependence of Saturation Magnetization upon Annealing Temperature

The saturation magnetization of SnO_2 samples annealed below 200 °C is low because there exists no ferromagnetism. Below 200 °C the nanoparticles are encapsulated by organic, e.g. acetate, coating from initial chemicals used for sol–gel reactions, which suppresses the formation of oxygen vacancies. These acetates are fully removed in the annealing process from 200 to 400 °C, as confirmed by thermogravimetric analysis [13]. Oxygen vacancies, including oxygen vacancies, can progressively appear on the surface of the nanoparticle, as the annealing temperature is increased. Accordingly, the saturation magnetization for SnO_2 nanoparticles increases with annealing temperature, and attains its maximum at 600 °C, as seen from Fig. 4 for SnO_2. Annealing above 600 °C, antiferromagnetic clusters form, which leads to a decrease in the saturation magnetization [9].

9 Concluding Remark

The EPR investigations of Co^{2+}-, Fe^{3+}-, Cr^{3+}-doped SnO_2 nanoparticles Ni^{2+}-, and Co^{2+}-doped CeO_2, and Fe^{3+}-doped ZnO nanoparticles for $\leq$5 % doping reveal the following features:

1. There occurs coexistence of bulk ferromagnetic phase due to ferromagnetic ordering of impurity transition-metal ions, which manifests as a broad FMR line in the EPR spectrum, and a paramagnetic phase due to localized moments of impurity paramagnetic TM ions, which exhibit narrow EPR lines. The saturation magnetization of these nanoparticles is proportional to the integrated intensity of the FMR line.
2. As yet, there is available no definitive explanation for the origin of ferromagnetism in oxide semiconductor nanoparticles. More experiments, including EPR/FMR, are required to understand it. However, the leading role of surface oxygen vacancies has been definitely established as one of the mechanisms for the origin of ferromagnetism.

3. The EPR spectrum in the core of a nanoparticle due to impurity ions is, in general, similar to that in the single crystal of the same compound. On the other hand, the EPR spectrum of the impurity ions located near or on the surface, enriched with oxygen vacancies, is different from that in the core area.
4. The method of synthesis, surface properties, and size of nanoparticles influence significantly the magnetic properties of DMS nanoparticles.
5. The saturation magnetization depends on annealing temperature. It increases with increasing annealing temperature, and attaining its maximum at 600 °C for SnO_2 samples. This is due to the progressive formation of oxygen vacancies on the nanoparticle surface, as the annealing temperature is increased to 600 °C. The saturation magnetization decreases above this temperature.
6. The saturation magnetization of nanoparticles depends on the amount of doping by impurities. Initially there occurs an increase of saturation magnetization with doping due to ions substituting at regular lattice sites, where the transition-metal impurity ions are coupled with each other via oxygen ions or oxygen vacancies. With further increase of doping the bulk ferromagnetism becomes suppressed due to redistribution of impurity ions inside the nanoparticle, and subsequent filling of interstitial positions instead of substitution at regular sites, which are no longer available.
7. The EPR spectrum depends significantly on the size of nanoparticle. There occurs a distribution of spin-Hamiltonian parameters in medium-size ($\sim$7 nm) nanoparticles due to the presence of defects and vacancies in the region intermediate to the surface and the core. For smaller nanoparticles (2.5–5 nm), ferromagnetic or superparamagnetic signals are observed at room temperature. Nanoparticles of size $\sim$25–40 nm exhibit distinct EPR/FMR spectra due to surface (ferromagnetic) and core (diamagnetic) regions. Larger nanoparticles, with size $>$40 nm exhibit spectra which are distinct from those with size $\leq$40 nm, because the core, which is a crystal-like part, becomes much larger, than the defect-enriched surface part of nanoparticle, and only EPR spectra of localized moments of transition-metal ions are detected there.

It is hoped that the review would lead to further planned research investigation of DMS oxides doped by TM ions for a better understanding of these materials and exploitation to fabricate spintronic devices.

Acknowledgments SKM is grateful to NSERC (Natural Sciences and Engineering Research Council of Canada) for partial financial support. SIA also acknowledges the support from the subsidy allocated to Kazan Federal University for performing the state assignment in the area of scientific activities.

References

1. J.M.D. Coey, M. Venkatesan, Half-metallic ferromagnetism: example of CrO_2 (invited). J. Appl. Phys. **91**, 8345–8350 (2002)
2. T. Dietl, H. Ohono, F. Matsukura, J. Cibert, D. Ferrand, Science **287**, 1019–1022 (2000)
3. X.X. Wei, C. Song, K.W. Geng, F. Zeng, B. He, F. Pan, J. Phys. Condens. Matter **18**, 7471–7479 (2006)

4. J.M.D. Coey, A.P. Douvalls, C.B. Fitzgerald, M. Venkatesan, Appl. Phys. Lett. **84**, 1332–1334 (2004)
5. A. Punnoose, J. Hays, A. Thurber, M.H. Engelhard, R.K. Kukkadapu, C. Wang, V. Shutthanandan, S. Thevuthasan, Phys. Rev. B **72**, 054402 (2005)
6. C. Van Komen, A. Thurber, K.M. Reddy, J. Hays, A. Punnoose, J. Appl. Phys. **103**, 07D141 (2008)
7. S.K. Misra, S.I. Andronenko, K. M. Reddy, J. Hays, A. Punnoose, J. Appl. Phys. **99**, 08 M106 (2006)
8. S.K. Misra, S.I. Andronenko, K.M. Reddy, J. Hays, A. Thurber, A. Punnoose, J. Appl. Phys. **101**, 09H120 (2007)
9. S.K. Misra, S.I. Andronenko, A. Punnoose, D. Tipikin, J.H. Freed, Appl. Magn. Reson. **36**, 291–295 (2009)
10. S.K. Misra, S.I. Andronenko, S. Rao, V.B. Bhat, C. Van Komen, A. Punnoose, J. Appl. Phys. **105**, 07C514 (2009)
11. S.K. Misra, S.I. Andronenko, M.E. Engelhard, A. Thurber, K.M. Reddy, A. Punnoose, J. Appl. Phys. **103**, 07D122 (2008)
12. A. Punnoose, K.M. Reddy, J. Hayes, A. Thurber, S. Andronenko, S.K. Misra, Appl. Magn. Reson. **36**, 331–345 (2009)
13. S.K. Misra, S.I. Andronenko, J.D. Harris, A. Thurber, G.L. Beausoleil II, A. Punnoose, J. Nanosci. Nanotechnol. **13**, 6798–6805 (2013)
14. S.K. Misra, S.I. Andronenko, A. Thurber, A. Punnoose, A. Nalepa, J. Magn. Magn. Mater. **363**, 82–87 (2014)
15. A. Prakash, S.K. Misra, D. Bahadur, Nanotechnology **24**, 095705 (2013)
16. M.B. Sahana, C. Sudakar, G. Setzler, A. Dixit, J.S. Thakur, G. Lawes, R. Naik, V.M. Naik, P.P. Vaishnava, Appl. Phys. Lett. **93**, 231909 (2008)
17. T.M. Hammad, J.K. Salem, R.G. Harrison, Appl. Nanosci. **3**, 133–139 (2013)
18. P. Jakes, E. Erdem, Physica status solidi (RRL) **5**, 56–58 (2011)
19. S.B. Orlinskii, J. Schmidt, P.G. Baranov, V. Lorrmann, D. Rauh, I. Riedel, V. Dyakonov, Phys. Rev. B **77**, 115334 (2008)
20. A. Thurber, K.M. Reddy, A. Punnoose, J. Appl. Phys. **101**, 09N506 (2007)
21. L.M. Johnson, A. Thurber, J. Anghel, M. Sabetian, M.H. Engelhard, D.A. Tenne, Ch.B. Hanna, A. Punnoose, Phys. Rev. B **82**, 054419 (2010)
22. S.B. Orlinskii, J. Schmidt, P.G. Baranov, D.M. Hofmann, C. de Mello Donegá, A. Meijerink, Phys. Rev. Lett. **92**, 047603 (2004)
23. S.B. Orlinskii, J. Schmidt, P.G. Baranov, C. de Mello Donegá, A. Meijerink, Phys. Rev. B **79**, 165316 (2009)
24. K.M. Whitaker, S.T. Ochsenbein, V.Z. Polinger, D.R. Gamelin, J. Phys. Chem. C **112**, 14331 (2008)
25. S.T. Ochsenbein, Y. Feng, K.M. Whitaker, E. Badaeva, W.K. Liu, X. Li, D.R. Gamelin, Nat. Nanotechnol. **4**, 681–687 (2009)
26. P.G. Baranov, S.B. Orlinskii, C. de Mello Donegá, J. Schmidt, Appl. Magn. Reson. **39**, 151–183 (2010)
27. P.G. Baranov, S.B. Orlinskii, C. de Mello Donegá, J. Schmidt, Phys. Status Sol. B **250**, 2137–2140 (2013)
28. A. Achkeev, I.R. Vakhitov, R.I. Khabibullin, L.R. Tagirov, J. Phys. Conf. Ser. **394**, 012018 (2012)
29. G.A. Alanko, A. Thurber, Ch. Hanna, A. Punnoose, J. Appl. Phys. **111**, 07C321 (2012)
30. A. Sundaresan, R. Bhargavi, N. Rangarajan, U. Siddesh, C.N.R. Rao, Phys. Rev. B **74**, 161306(R) (2006)
31. Q.Y. Wen, H.W. Zhang, Y.Q. Song, Q.H. Yang, H. Zhu, J.Q. Xiao, J. Phys. Condens. Matter **19**, 246205 (2007)
32. J.M.D. Coey, P. Stamenov, P.D. Gunning, M. Venkatesan, K. Paul, New J. Phys. **12**, 053025 (2010)
33. A. Mauger, Appl. Magn. Reson. **39**, 3–29 (2010)
34. A. Ney, A. Kovács, V. Ney, S. Ye, K. Ollefs, T. Kammermeier, F. Wilhelm, A. Rogalev, R.E. Dunin-Borkowski, New J. Phys. **13**, 103001 (2011)
35. N. Volbers, H. Zhou, C. Knies, D. Pfisterer, J. Sann, D.M. Hofmann, B.K. Meyer, Appl. Phys. A **88**, 153–155 (2007)
36. C. Morhain, C. Deparis, M. Laugt, M. Goiran, Z. Golacki, Phys. Rev. Lett. **96**, 017203 (2006)
37. S. D'Ambrosio, V. Pashchenko, J.-M. Mignot, O. Ignatchik, R.O. Kuzian, A. Savoyant, Z. Golacki, K. Grasza, A. Stepanov, Phys. Rev. B **86**, 035202 (2012)

38. D.V. Azamat, A. Dejneka, V.A. Trepakov, L. Jastrabik, M. Fanciulli, V.Y. Ivanov, M. Godlewski, V.I. Sokolov, J. Rosa, A.G. Badalyan, Phys. Status Solidi RRL **5**, 138–140 (2011)
39. O. Toulemonde, M. Gaudon, J. Phys. D Appl. Phys. **43**, 045001 (2010)
40. S.K. Misra, S. Diehl, J. Magn. Reson. **219**, 53–60 (2012)